

RSC Advances



This is an *Accepted Manuscript*, which has been through the Royal Society of Chemistry peer review process and has been accepted for publication.

Accepted Manuscripts are published online shortly after acceptance, before technical editing, formatting and proof reading. Using this free service, authors can make their results available to the community, in citable form, before we publish the edited article. This *Accepted Manuscript* will be replaced by the edited, formatted and paginated article as soon as this is available.

You can find more information about *Accepted Manuscripts* in the [Information for Authors](#).

Please note that technical editing may introduce minor changes to the text and/or graphics, which may alter content. The journal's standard [Terms & Conditions](#) and the [Ethical guidelines](#) still apply. In no event shall the Royal Society of Chemistry be held responsible for any errors or omissions in this *Accepted Manuscript* or any consequences arising from the use of any information it contains.

1 **Adsorption behavior of Cr(VI) from aqueous solution onto magnetic graphene**
2 **oxide functionalized with 1,2-diaminocyclohexanetetraacetic acid**

3

4 Fang-ying Guo^{a,b}, Yun-guo Liu^{a,b,*}, Hui Wang^{a,b}, Guang-ming Zeng^{a,b}, Xin-jiang Hu^{a,b},
5 Bo-hong Zheng^c, Ting-ting Li^{a,b}, Xiao-fei Tan^{a,b}, Shu-fan Wang^{a,b}, Ming-ming
6 Zhang^{a,b}

7

8 ^a College of Environmental Science and Engineering, Hunan University, Changsha
9 410082, PR China

10 ^b Key Laboratory of Environmental Biology and Pollution Control (Hunan
11 University), Ministry of Education, Changsha 410082, PR China

12 ^c School of Architecture and Art, Central South University, Changsha 410082, PR
13 China

14

15 *Corresponding author: Yun-guo Liu; Tel.: + 86 731 88649208; Fax: + 86 731
16 88822829; E-mail address: nhxyhj111@163.com

17

18 Abstract

19 A novel magnetic composite adsorbent was synthesized by grafting
20 1,2-diaminocyclohexanetetraacetic acid to magnetic graphene oxide (DCTA/E/MGO).
21 The DCTA/E/MGO was employed for removing Cr(VI) from aqueous solution in this
22 study. The composite was characterized by FESEM, TEM, BET, XRD, FT-IR and
23 XPS. The adsorption behaviors of Cr(VI) by the DCTA/E/MGO in aqueous solution
24 were systematically investigated. Second order kinetic and Freundlich isotherm
25 models validated the experimental data. The adsorption rate was influenced by both
26 film diffusion and intraparticle diffusion. Thermodynamic parameters revealed that
27 the adsorption reaction was an endothermic and spontaneous process. The novel
28 adsorbent exhibited better Cr(VI) removal efficiency in solutions with low pH. The
29 decontamination of Cr(VI) by DCTA/E/MGO was influenced by ionic strength. These
30 results are important for estimating and optimizing the removal of metal ions by
31 DCTA/E/MGO composite.

32 **Keywords:** 1,2-diaminocyclohexanetetraacetic acid; Ethylenediamine; Magnetic
33 graphene oxide; Cr(VI); Removal

34 1. Introduction

35 Chromium is usually found in two common oxidation states, Cr(VI) and Cr(III).
36 Usually Cr(VI) compounds are more toxic than Cr(III) because of their marked
37 carcinogenic, teratogenic and mutagenic effects to human and other living organisms.¹
38 Thus, it is necessary to remove Cr(VI) contaminants from wastewater before being

39 released into the environment. Various methods of chromium removal have been well
40 documented, including ion exchange, evaporation, chemical precipitation, membrane
41 separation, adsorption, etc.² Among all of these methods, adsorption is one of the
42 most economically favorable and technically easy methods.³

43 Normally, the adsorption ability of a material is controlled in part by the number
44 of available functional groups. Graphene oxide (GO) prepared by Hummers method⁴
45 contains a range of oxygen-containing functional groups on the surface, such as
46 hydroxyl, epoxide, carbonyl and carboxyl groups.⁵ These groups are available for
47 removing heavy metals from wastewater. In addition, GO is characterized by a large
48 specific surface area and can be readily obtained from cheap natural graphite in large
49 scale.⁶ From these points, GO is considered as a suitable adsorbent for the removal of
50 pollutants in water. However, GO can be dispersed in aqueous media due to the
51 oxygen-containing functional groups on its surface, therefore it is difficult to be
52 separated from water after the adsorption process. The problem can be solved by
53 loading magnetic nanoparticles to GO. The separation can be achieved by magnetic
54 separation. The magnetic technology combines the advantages of adsorption with the
55 merit of easy separation, but it has been found to have some negative effects on the
56 adsorption capacity of the GO.^{7, 8}

57 In order to improve the adsorption ability and selectivity of GO for metal ions, a
58 great number of GO derivatives have been obtained by grafting new chemical
59 substances on the GO backbone, such as sulfanilic acid,⁴ EDTA,⁵ chitosan⁹ and
60 ethylenediamine¹⁰. Meanwhile, 1,2-diaminocyclohexane-N,N,N',N'-tetraacetic acid

61 (DCTA), acting as a multidentate chelating ligand, can form strong complexes with
62 most metals. These complexes have similar chemical structures to those formed with
63 ethylenediaminetetraacetic acid (EDTA) but have higher stability constants for most
64 metals.^{11, 12} Besides, among various functional groups, the amine group has a
65 relatively high reactivity and can easily react with many chemicals.^{2, 8} Therefore, it is
66 a feasible way to graft DCTA onto magnetic graphene oxide (MGO) through the
67 ethylenediamine.

68 The main objectives of this work were to: (1) prepare DCTA/E/MGO composite
69 and characterize it by FESEM, TEM, BET, XRD, FT-IR and XPS; (2) study the
70 adsorption mechanism with kinetics, isotherm and thermodynamic models; (3)
71 evaluate the effects of process parameters on Cr(VI) removal, i.e., pH, initial ion
72 concentrations and temperature; (4) investigate the effects of ionic strength on Cr(VI)
73 decontamination.

74 **2. Materials and methods**

75 2.1. Materials

76 Graphite powder was supplied by Tianjin Hengxin Chemical Preparation Co.,
77 Ltd., China. 1,2-diaminocyclohexane-N,N,N',N'-tetraacetic acid (DCTA) was
78 purchased from Xiya Reagent Research Center (Shandong, China). Ethylenediamine
79 was purchased from Shanghai Chemical Reagents Factory. The reagents
80 1-ethyl-3-(3-dimethylaminopropyl) carbodiimide hydrochloride (EDC), N-hydroxyl
81 succinimide (NHS) were obtained from Shanghai Civi Chemical Technology Co., Ltd.,

82 China. All chemicals used in the experiments were analytical grade.

83 GO was synthesized via modified Hummers method¹³ from the natural graphite
84 powder. Briefly, graphite powders were first oxidized by concentrated H₂SO₄, K₂S₂O₈
85 and P₂O₅. Next, the concentrated H₂SO₄, KMnO₄ and NaNO₃ were used to oxidize the
86 preoxidized graphite, then 30% H₂O₂ was added to eliminate the excess MnO₄⁻, and
87 the products were rinsed with HCl (10%) and Milli-Q water. The resulting solution
88 was sonicated for 2 h. The magnetic graphene oxide (MGO) was prepared by
89 coprecipitation method. Fe³⁺ and Fe²⁺ (molar ratio 2:1) were mixed in the GO solution
90 with addition of ammonia solution to form Fe₃O₄-GO composite.^{4, 14}

91 The DCTA/E/MGO was prepared by reacting DCTA with MGO through
92 ethylenediamine. 0.1 M EDC and 0.1 M NHS solution were added to the DCTA
93 dispersion with continuous stirring for 2 h,^{15, 16} then ethylenediamine was added. The
94 mixed system was stirred continuously for 6 h in a water bath at 80 °C after being
95 added into MGO dispersion.^{8, 15} The resulted product was washed repeatedly with
96 Milli-Q water until pH was about neutral and finally stored at room temperature. The
97 preparation sketch of DCTA/E/MGO is shown in Fig. 1.

98 2.2. Characterization

99 The morphology of the as-prepared adsorbent was characterized by
100 field-emission scanning electron microscopy (FESEM, JSM 6700F, Japan) and
101 transmission electron microscopy (TEM, Tecnai G2 F20, USA). The BET specific
102 surface area was determined using nitrogen adsorption-desorption measurements

103 (Autosorb-1, Quantachrome Instruments, USA). The X-ray diffraction (XRD) patterns
104 of GO, MGO and DCTA/E/MGO composite were obtained on an X-ray diffractometer
105 (Rigaku D/max-2500, Japan) with CuK α radiation. The FT-IR spectra of the
106 DCTA/E/MGO and MGO were measured on a spectrophotometer (Varian 3100, USA)
107 using the KBr pellet technique. The XPS measurements were performed using an
108 ESCALAB 250Xi X-ray photoelectron spectrometer (Thermo Fisher, USA).

109 2.3. Adsorption experiments

110 A stock solution of Cr(VI) was prepared by dissolving 2.8287 g of 99.9%
111 potassium dichromate (K₂Cr₂O₇) in 1000 mL of distilled water. The solutions of
112 different Cr(VI) concentrations used in batch experiments were obtained by diluting
113 the stock solution. All batch adsorption experiments were performed on an orbital
114 shaker with a shaking speed of 150 rpm. For all the adsorption experiments, the
115 suspension of MGO or DCTA/E/MGO was added to achieve the expected
116 concentrations of the different components. Initial pH values of the Cr(VI) solutions
117 were adjusted to the desired pH by adding negligible volumes of NaOH or HNO₃.
118 After the adsorption process, the mixture was conveniently separated by a permanent
119 magnet. The concentration of Cr(VI) in the supernatant was determined on a UV-vis
120 spectrophotometer. The Cr(VI) removal at the equilibrium (q_e (mg/g)) was calculated
121 as follows:

$$122 \quad q_e = \frac{(C_0 - C_e)V}{W} \quad (1)$$

123 where, C_0 and C_e (mg/L) are the initial and equilibrium concentrations of Cr(VI) ions,

124 respectively; V is the volume of the solution (L); and W is the amount of adsorbent
125 (g).

126 3. Results and discussion

127 3.1. Characterization of DCTA/E/MGO

128 The FESEM and TEM images of DCTA/E/MGO are demonstrated in Fig. 2.
129 These images show that Fe_3O_4 particles are dispersed on the surface and some
130 wrinkles are observed. The surface of the composite is rough, which can indicate an
131 excellent possibility for the heavy metals to be trapped and adsorbed by the
132 DCTA/E/MGO.

133 The N_2 adsorption – desorption isotherms (in Fig.3a) were recorded to
134 investigate the BET surface areas and pore structure of MGO and DCTA/E/MGO
135 composite. The BET surface area of the DCTA/E/MGO was measured to be 310.41
136 $\text{m}^2 \text{g}^{-1}$, which is much higher than that of MGO ($114.61 \text{ m}^2 \text{g}^{-1}$). Nitrogen adsorption
137 – desorption analysis shows all the DCTA/E/MGO and MGO samples with micro-
138 and meso-porous structure. The pore size of DCTA/E/MGO samples mainly distribute
139 at 1.4 nm (Fig. 3b). The introduction of DCTA led to a distinct increase in BET
140 surface area which is beneficial for adsorption.

141 The XRD patterns of GO, MGO and DCTA/E/MGO are shown in Fig. 3c and d.
142 For GO, a strong peak at $2\theta = 10.4^\circ$ occurs, which is the structure expansion as
143 oxygen-containing groups incorporate between the carbon sheets during the course of
144 strong oxidation. For MGO and DCTA/E/MGO, the intense diffraction peaks at the

145 Bragg angles of 30.09, 35.42, 37.05, 43.05, 53.39, 56.94 and 62.51 were observed
146 clearly. These peaks are consistent with the (220), (311), (222), (400), (422), (511)
147 and (440) facets of the cubic spinel crystal planes of Fe_3O_4 (JCPDS card No. 19-0629),
148 respectively.¹⁷ Compared with the pure GO diffracted signals, there are no diffracted
149 signals for the GO sheets in MGO and DCTA/E/MGO, which is ascribed to that the
150 strong signals of the iron oxides tend to overwhelm the weak carbon peaks.¹⁸ Almost
151 similar XRD patterns of MGO and DCTA/E/MGO were observed, which revealed
152 that the synthesized process did not change the crystalline phase of Fe_3O_4 . But, it was
153 not sufficient to exclude the existence of $\gamma\text{-Fe}_2\text{O}_3$. However, the magnetic properties
154 of $\gamma\text{-Fe}_2\text{O}_3$ are similar to Fe_3O_4 , so there was no negative impact on the following
155 experiments whether $\gamma\text{-Fe}_2\text{O}_3$ was contained in the samples or not.¹⁹

156 The FT-IR spectra of MGO and DCTA/E/MGO in the range of 4000–500 cm^{-1}
157 are shown in Fig. 3e. The FTIR spectra of MGO and DCTA/E/MGO show the
158 presence of O–H at 3449 cm^{-1} . In the FT-IR spectrum of MGO, the peak at 1730 cm^{-1}
159 corresponding to C=O of carboxyl group on the GO shifts to 1643 cm^{-1} may be due to
160 the formation of -COO^- after coating with Fe_3O_4 .⁴ The stretching band of Fe–O peak
161 appears at around 580 cm^{-1} . While in the FT-IR spectrum of DCTA/E/MGO, the
162 bands at 1636 and 1616 cm^{-1} correspond to the characteristic C=O stretching
163 vibration of -NHCO- (amide I) and the N–H bending of -NH_2 , respectively.^{8,20} The
164 peaks at 1035 and 1384 cm^{-1} correspond to C–O–C stretching vibration and C–OH
165 stretching, respectively.¹⁷ After the chemical grafting, the bands at 1636 and 1616
166 cm^{-1} appeared, demonstrating that DCTA and ethylenediamine were successfully

167 grafted on MGO.

168 The chemical state of element in MGO and DCTA/E/MGO was further
169 investigated by XPS. The wide scan XPS spectrum (Fig. 3f) of DCTA/E/MGO shows
170 photoelectron lines at binding energies of about 285, 400, 530, and 711 eV which are
171 attributed to C1s, N1s, O1s, and Fe2p, respectively.²¹ The XPS survey of
172 DCTA/E/MGO indicates significant amount of N1s comparing to that of MGO (Fig.
173 3f), which is originated from the grafted ethylenediamine and DCTA. The elemental
174 analysis illustrates a considerable increase in O/C atomic ratio in the DCTA/E/MGO
175 (0.44) comparing to that of the MGO (0.31), which may be attributed to the high O/C
176 atomic ratio of the introduced DCTA. In addition, five different peaks (Fig. 3g)
177 centered at 284.6 eV, 286.3 eV, 286.9 eV, 288.2 eV and 289.0 eV are observed,
178 corresponding to C-C, C-O, C-O-C, C=O and O-C=O groups of MGO,
179 respectively.²² The C1s spectrum of DCTA/E/MGO (Fig. 3h) can be curve-fitted into
180 five peak components with binding energies of about 284.6, 285.6, 286.5, 287.5 and
181 288.9 eV, which attribute to the carbon atoms in the forms of C-C, C-N, C-O,
182 HNC=O and O-C=O species, respectively.^{8, 23, 24} Additional C-N and HNC=O
183 species functions are observed. Thus, it can be concluded that DCTA has been grafted
184 successfully to the MGO surface.

185 3.2. Adsorption kinetics

186 The adsorption kinetics is an important parameter for determination of the
187 optimum adsorption time. The kinetic studies for Cr(VI) adsorption on the

188 DCTA/E/MGO were carried out at three different Cr(VI) concentrations (10, 20, and
189 40 mg/L) and the results are given in Fig. 4a. It is shown that the amount of adsorbed
190 Cr(VI) increased rapidly over the first 6 h of contact time. Furthermore, three kinetic
191 models were tested to analyze the adsorption process, including pseudo-first-order
192 kinetic model, pseudo-second-order kinetic model and intraparticle diffusion model.
193 Fig. 4b and c show the pseudo-first-order and pseudo-second-order kinetics for the
194 adsorption of Cr(VI) onto DCTA/E/MGO, respectively. These two kinetic models can
195 be expressed as follows²⁵:

$$196 \quad \log(q_e - q_t) = \log(q_e) - \frac{k_1 t}{2.303} \quad (2)$$

$$197 \quad \frac{t}{q_t} = \frac{1}{k_2 q_e^2} + \frac{t}{q_e} \quad (3)$$

198 where k_1 is the rate constant of pseudo-first-order adsorption (1/min); k_2 is the rate
199 constant of pseudo-second-order adsorption (g/mg min); q_e and q_t are the amounts of
200 Cr(VI) adsorbed at equilibrium and at any time t , respectively (mg/g).

201 The kinetic parameters calculated from the two models are listed in Table 1.
202 From Table 1, it is noticed that the R^2 values of pseudo-second-order model (0.999,
203 0.998, and 0.998) are higher than those of pseudo-first-order model (0.894, 0.911, and
204 0.955). In addition, the calculated q_e values of the pseudo-second-order model agree
205 with the experimental data better than those of the pseudo-first-order model. Based on
206 these data, it can be concluded that the Cr(VI) uptake process complies with the
207 second-order type kinetic reaction, which indicates that the rate-limiting step may be
208 due to the chemical adsorption, high specific surface area and the absence of internal
209 diffusion resistance.^{8,26,27} It is also notable that the constant rate k_2 decreases with the

210 increase of initial Cr(VI) concentration, which may be connected with the longer time
211 required to reach the equilibrium state.²⁸

212 To highlight the influence of diffusion on the adsorption mechanism of Cr(VI),
213 the kinetic data were analyzed by applying the intraparticle diffusion model, which
214 can be described as follows²⁹:

$$215 \quad q_t = K_d t^{0.5} + I \quad (4)$$

216 where q_t (mg/g) is the adsorption capacity at time t ; K_d is the intraparticle diffusion
217 rate constant (mg/g min^{1/2}); I is a constant that gives idea about the thickness of the
218 boundary layer. The larger value of I , the greater the boundary layer effect will be.³⁰

219 If the plot q_t versus $t^{0.5}$ is linear and passes through the origin, the intraparticle
220 diffusion is the only rate-limiting step; if the plot presents multilinearity, the
221 adsorption process is controlled by two or more steps.²⁸ As can be seen from Fig. 4d,
222 there are three processes controlling the adsorption rate: (i) the first sharper portions
223 may be attributed to the film diffusion; (ii) the second linear portions are the gradual
224 adsorption stages, where the intra-particle diffusion is rate-controlling step; and (iii)
225 the third portions are final equilibrium stages where intra-particle diffusion starts to
226 slow down due to low adsorbate concentration in aqueous solution as well as less
227 number of available adsorption sites.³¹ Therefore, the overall rate-limiting step
228 involves both film diffusion and intraparticle diffusion.

229 3.3. Adsorption isotherm and thermodynamics

230 The equilibrium adsorption isotherm is studied in detail, since it could provide

231 information about the surface properties of adsorbent and the adsorption behavior. In
232 this work, the adsorption isotherms of Cr(VI) were investigated at 288, 303 and 318 K,
233 respectively. Since Langmuir and Freundlich isotherm models are commonly used in
234 description of liquid–solid systems, they were applied to simulate the experimental
235 data of the adsorption processes.³² The Langmuir model is based on the assumption
236 that monolayer surface adsorption occurs on specific homogeneous sites without any
237 interaction between the adsorbed pollutants.³³ The equation is commonly described
238 as³⁴:

$$239 \quad q_e = \frac{K_L q_m C_e}{1 + K_L C_e} \quad (5)$$

240 where C_e is the equilibrium concentration (mg/L); q_e is the amount of metal ion
241 adsorbed (mg/g); q_m is the theoretical saturation capacity of the monolayer (mg/g); K_L
242 is a constant related to the affinity of the binding sites (L/mg). The Freundlich model
243 assumes the adsorption on a heterogeneous surface without saturation of adsorbent
244 binding sites. It can be represented by the following equation³⁵:

$$245 \quad q_e = K_F C_e^{\frac{1}{n}} \quad (6)$$

246 where K_F (mg/g) is a unit capacity coefficient and n is the Freundlich parameter
247 related to the intensity of adsorption, which varies with the heterogeneity of the
248 material. If n values are in the range $1 < n < 10$, the adsorption process is favourable,
249 then the adsorption capacity increases and new adsorption sites occur.^{36, 37}

250 The Langmuir and Freundlich adsorption isotherms obtained using the nonlinear
251 method are shown in Fig. 5, and the related parameters of the two models are listed in
252 Table 2. From the correlation coefficients (R^2) and the fitting curves, the experimental

253 data are fitted better by the Freundlich model than by the Langmuir model within the
254 studied temperature range. The better fitting of the Freundlich isotherm indicates that
255 the surface of the DCTA/E/MGO is likely to be heterogeneous. Moreover, all the
256 values of Freundlich constant n (Table 2) in this study are within the beneficial
257 adsorption range, which indicates that the DCTA/E/MGO composite can be used as an
258 effective adsorbent.

259 The thermodynamic parameters provide in-depth information about internal
260 energy changes that are associated with adsorption. The standard free-energy change
261 (ΔG°), the standard enthalpy change (ΔH°), and the standard entropy change (ΔS°)
262 are calculated from the temperature-dependent adsorption isotherms to evaluate the
263 feasibility and exothermic nature of the adsorption process. These parameters can be
264 calculated using the following equations:

$$265 \quad \Delta G^\circ = -RT \ln K^\circ \quad (7)$$

$$266 \quad \ln K^\circ = -\frac{\Delta H^\circ}{RT} + \frac{\Delta S^\circ}{R} \quad (8)$$

267 where R (8.314 J/mol K) is the universal gas constant, T (K) is the absolute
268 temperature and K° could be calculated by plotting $\ln K_d$ ($K_d = q_e/C_e$) versus C_e and
269 extrapolating C_e to zero.³⁸ The values of ΔH° and ΔS° were calculated from the slope
270 and intercept of a plot of $\ln K^\circ$ against $1/T$. The calculated results are given in Table 3.

271 The ΔG° values are negative, which indicated the spontaneity of the adsorption
272 process. Values of ΔG° decreased slightly with the increase of temperature, which
273 revealed the improvement of the adsorption by increasing the temperature. The
274 positive ΔH° value suggested the endothermic nature of adsorption, which agreed well

275 with the result that the adsorption of Cr(VI) increased along with the increase of
276 temperature (Fig. 4). In addition, the positive ΔS° indicated that the degrees of
277 freedom increased at the solid–liquid interface during the adsorption process.³

278 3.4. Effect of the solution pH.

279 Solution pH is a significant controlling factor in adsorption process due to its
280 effect on surface charge of the adsorbent, speciation of adsorbate and the degree of
281 ionization.³⁸ The adsorption of Cr(VI) onto DCTA/E/MGO and MGO as functions of
282 solution pH is presented in Fig. 6a. The results indicate that the adsorption of Cr(VI)
283 shows strong dependence on solution pH. The adsorption capacities of DCTA/E/MGO
284 and MGO for Cr(VI) are found to decrease drastically with the increase of pH ranging
285 from 2.0 to 9.0. Other workers have reported similar phenomena for the removal of
286 Cr(VI) by modified GO.^{17, 39}

287 In aqueous solutions, Cr(VI) exists in different ionic forms such as chromate
288 (CrO_4^{2-}), dichromate ($\text{Cr}_2\text{O}_7^{2-}$) and hydrogen chromate (HCrO_4^-), depending on the
289 solution pH and the Cr(VI) concentration.¹ In the pH range of 1.0–6.0, HCrO_4^- is the
290 predominant Cr(VI) species. As pH increases, the predominant species is CrO_4^{2-} .³ At
291 low pH, the large number of protons can easily coordinate with the functional groups
292 on the material surface, which makes the material surface more positive. Thus, higher
293 adsorption capacity at low pH can be explained by the strong electrostatic attraction
294 between the positively charged adsorbent surface and the negatively charged
295 chromate ions. Besides, lower adsorption capacity of Cr(VI) in high pH environment

296 may be due to the dual competition of the anions (CrO_4^{2-} and OH^-) adsorbed on the
297 surface of the adsorbent.⁴⁰

298 The q_{max} value of Cr(VI) adsorption on DCTA/E/MGO is about 80 mg/g, which
299 is obviously higher than that of MGO (48 mg/g) and other adsorbents, such as
300 ethylenediamine functionalized Fe_3O_4 (61.35 mg/g),²⁷ magnetic cyclodextrin–
301 chitosan/graphene oxide (67.66 mg/g)¹⁷ and cyclodextrin/ethylenediamine/magnetic
302 graphene oxide (68.41 mg/g).⁸ It can be seen that the DCTA/E/MGO has higher
303 sorption capacity. DCTA and ethylenediamine have two types of reactive functional
304 groups, carboxyl groups and amino groups, which act as chelation sites and increase
305 the adsorption capacity.

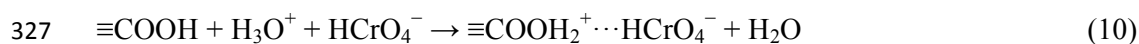
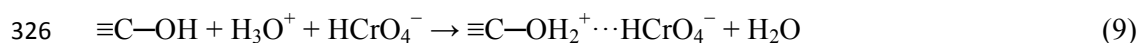
306 3.5. Effect of ionic strength.

307 The effect of ionic strength on the adsorption of Cr(VI) on DCTA/E/MGO was
308 studied by carrying out a series of experiments at three different NaCl concentrations.
309 As seen from Fig. 6b, the adsorption of Cr(VI) on DCTA/E/MGO decreased as the
310 NaCl concentration ranked from 0.002 to 0.2 M. This phenomenon can be attributed
311 to the following three reasons: (1) competition of Cl^- with Cr(VI) for the adsorption
312 sites on DCTA/E/MGO results in the decrease of the uptake capacity.⁸ (2) the increase
313 in NaCl concentration increases the screening effect between the negatively charged
314 Cr(VI) in solution and the positively charged adsorbent surface.⁴¹ (3) increased ionic
315 strength reduces electrostatic repulsion, thereby increasing DCTA/E/MGO particle
316 aggregation. These effects reduce the amount of available binding sites and also

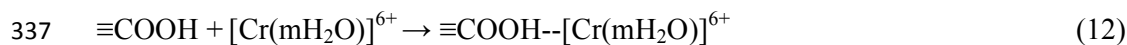
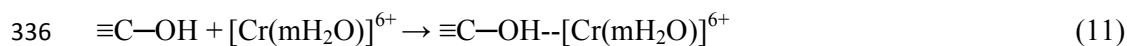
317 decrease the adsorption of Cr(VI).⁴²

318 3.6. Proposed mechanisms of adsorption

319 According to the above theories and discussions, we can get that both
 320 chemisorption and physisorption are involved in the Cr(VI) adsorption process. The
 321 adsorption of Cr(VI) onto DCTA/E/MGO may be attributed to surface electrostatic
 322 attraction, coordination and hydrogen bonding. The first possible mechanism is
 323 adsorption by electrostatic forces of the protonated sites ($-\text{OH}_2^+$ and $-\text{COOH}_2^+$) on the
 324 DCTA/E/MGO surface and the negative charge of the HCrO_4^- , which results in
 325 complex formation.⁴³ The possible reactions are shown in Eqs. (9) and (10).



328 where $\equiv\text{C}$ represents the surface of DCTA/E/MGO. Besides, the DCTA grafted on the
 329 MGO surface can form complexes with Cr(VI) ions by chelation. The hydroxyl
 330 groups and nitrogen groups on the surfaces of DCTA/E/MGO have lone pairs of
 331 electrons for donation, and the Cr(VI) have vacant orbitals that can accept electron
 332 pairs from donor atoms and form coordinate covalent bonds. In addition to the above
 333 two possible mechanisms, another mechanism of adsorption of Cr(VI) on
 334 DCTA/E/MGO may involve the interaction between HCrO_4^- and surface groups of
 335 DCTA/E/MGO by the formation of hydrogen bonding.^{8, 38}



338 4. Conclusions

339 The analysis results of FESEM, TEM, BET, XRD, FT-IR and XPS indicated that
340 the DCTA/E/MGO composite was successfully prepared and it was more effective for
341 Cr(VI) removal from water. The adsorption followed pseudo-second-order kinetic
342 model. The equilibrium data were well-modeled by the Freundlich isotherm model.
343 Decontamination of Cr(VI) was found to be more effective at higher temperature and
344 lower pH range. Besides, the presence of NaCl in the solution has a negative influence
345 on the adsorption process. Adsorption mechanisms proposed in this study included the
346 electrostatic interaction, coordination and hydrogen bonding. In summary, the novel
347 DCTA/E/MGO composite can be utilized as an efficient adsorbent for the Cr(VI)
348 removal.

349 Acknowledgements

350 The authors would like to thank financial support from the National Natural
351 Science Foundation of China (Grant No. 41271332 and 51478470) and the Hunan
352 Provincial Innovation Foundation For Postgraduate (Grant No. CX2012B138).

353 References

- 354 1. W. Liu, J. Zhang, C. Zhang and L. Ren, *Chem. Eng. J.*, 2012, 189-190,
355 295-302.
- 356 2. S. Luo, X. Xu, G. Zhou, C. Liu, Y. Tang and Y. Liu, *J. Hazard. Mater.*, 2014,
357 274, 145-155.

- 358 3. X. J. Hu, J. S. Wang, Y. G. Liu, X. Li, G. M. Zeng, Z. L. Bao, X. X. Zeng, A.
359 W. Chen and F. Long, *J. Hazard. Mater.*, 2011, 185, 306-314.
- 360 4. X.-j. Hu, Y.-g. Liu, H. Wang, A.-w. Chen, G.-m. Zeng, S.-m. Liu, Y.-m. Guo,
361 X. Hu, T.-t. Li, Y.-q. Wang, L. Zhou and S.-h. Liu, *Sep. Purif. Technol.*, 2013,
362 108, 189-195.
- 363 5. C. J. Madadrang, H. Y. Kim, G. Gao, N. Wang, J. Zhu, H. Feng, M. Gorrington,
364 M. L. Kasner and S. Hou, *ACS Appl. Mater. Interfaces*, 2012, 4, 1186-1193.
- 365 6. S. Stankovich, D. A. Dikin, G. H. Dommett, K. M. Kohlhaas, E. J. Zimney, E.
366 A. Stach, R. D. Piner, S. T. Nguyen and R. S. Ruoff, *Nature*, 2006, 442,
367 282-286.
- 368 7. J. Li, S. Zhang, C. Chen, G. Zhao, X. Yang, J. Li and X. Wang, *ACS Appl.*
369 *Mater. Interfaces*, 2012, 4, 4991-5000.
- 370 8. H. Wang, Y. G. Liu, G. M. Zeng, X. J. Hu, X. Hu, T. T. Li, H. Y. Li, Y. Q.
371 Wang and L. H. Jiang, *Carbohydr. Polym.*, 2014, 113, 166-173.
- 372 9. L. Fan, C. Luo, M. Sun, X. Li and H. Qiu, *Colloids Surf. B, Biointerfaces*,
373 2013, 103, 523-529.
- 374 10. H.-L. Ma, Y. Zhang, Q.-H. Hu, D. Yan, Z.-Z. Yu and M. Zhai, *J. Mater. Chem.*,
375 2012, 22, 5914-5916.
- 376 11. E. A. Gautier, R. T. Gettar, R. E. Servant and D. A. Batistoni, *J. Chromatogr. A*,
377 1995, 706, 115-119.
- 378 12. E. Norkus, J. Vaičiūnienė and T. Vuorinen, *Carbohydr. Polym.*, 2006, 66,
379 316-320.

- 380 13. S. T. Yang, Y. Chang, H. Wang, G. Liu, S. Chen, Y. Wang, Y. Liu and A. Cao, *J.*
381 *Colloid Interface Sci.*, 2010, 351, 122-127.
- 382 14. X.-j. Hu, Y.-g. Liu, H. Wang, G.-m. Zeng, X. Hu, Y.-m. Guo, T.-t. Li, A.-w.
383 Chen, L.-h. Jiang and F.-y. Guo, *Chem. Eng. Res. Des.*, 2015, 93, 675-683.
- 384 15. D. Depan, B. Girase, J. S. Shah and R. D. Misra, *Acta Biomater.*, 2011, 7,
385 3432-3445.
- 386 16. C. L. Lulu Fan, Min Sun, Xiangjun Li, Fuguang Lu, Huamin Qiu, *Bioresour.*
387 *Technol.*, 2012, 114, 703-706.
- 388 17. L. Li, L. Fan, M. Sun, H. Qiu, X. Li, H. Duan and C. Luo, *Colloids Surf. B,*
389 *Biointerfaces*, 2013, 107, 76-83.
- 390 18. H. Wang, X. Yuan, Y. Wu, X. Chen, L. Leng, H. Wang, H. Li and G. Zeng,
391 *Chem. Eng. J.*, 2015, 262, 597-606.
- 392 19. M. Zhang, Y. Wang, X. Jia, M. He, M. Xu, S. Yang and C. Zhang, *Talanta,*
393 2014, 120, 376-385.
- 394 20. D. Sebben and P. Pendleton, *Spectrochim. Acta A: Mol. Biomol. Spectrosc.*,
395 2014, 132, 706-712.
- 396 21. T. Siva, K. Kamaraj, V. Karpakam and S. Sathiyarayanan, *Prog. Org. Coat.*,
397 2013, 76, 581-588.
- 398 22. J. Liu, G. Chen and M. Jiang, *Macromolecules*, 2011, 44, 7682-7691.
- 399 23. X. Song, Y. Yang, J. Liu and H. Zhao, *Langmuir*, 2011, 27, 1186-1191.
- 400 24. H. Min, P. L. Girard-Lauriault, T. Gross, A. Lippitz, P. Dietrich and W. E.
401 Unger, *Anal. Bioanal. Chem.*, 2012, 403, 613-623.

- 402 25. J. L. Gong, B. Wang, G. M. Zeng, C. P. Yang, C. G. Niu, Q. Y. Niu, W. J. Zhou
403 and Y. Liang, *J. Hazard. Mater.*, 2009, 164, 1517-1522.
- 404 26. W. Plazinski, W. Rudzinski and A. Plazinska, *Adv. Colloid Interface Sci.*, 2009,
405 152, 2-13.
- 406 27. Y. G. Zhao, H. Y. Shen, S. D. Pan and M. Q. Hu, *J. Hazard. Mater.*, 2010, 182,
407 295-302.
- 408 28. C. Balan, I. Volf and D. Bilba, *Chem. Ind. Chem. Eng. Q.*, 2013, 19, 615-628.
- 409 29. A. L. ZA, M. Naushad and R. Ali, *Environ. Sci. Pollut. Res. Int.*, 2013, 20,
410 3351-3365.
- 411 30. L. Zhang, X. Q. Jiang, T. C. Xu, L. J. Yang, Y. Y. Zhang and H. J. Jin, *Ind. Eng.*
412 *Chem. Res.*, 2012, 51, 5577-5584.
- 413 31. J. Lin, Y. Zhan and Z. Zhu, *Colloids Sur. A: Physicochem. Eng. Asp.*, 2011,
414 384, 9-16.
- 415 32. D. G. Kinniburgh, *Environ. Sci. Technol.*, 1986, 20, 895-904.
- 416 33. L. Wang, W. Liu, T. Wang and J. Ni, *Chem. Eng. J.*, 2013, 225, 153-163.
- 417 34. X. Mi, G. Huang, W. Xie, W. Wang, Y. Liu and J. Gao, *Carbon*, 2012, 50,
418 4856-4864.
- 419 35. E. Repo, J. K. Warchol, T. A. Kurniawan and M. E. T. Sillanpää, *Chem. Eng.*
420 *J.*, 2010, 161, 73-82.
- 421 36. S. Basha and Z. V. P. Murthy, *Process Biochem.*, 2007, 42, 1521-1529.
- 422 37. C. H. Wu, *J. Hazard. Mater.*, 2007, 144, 93-100.
- 423 38. J. Xu, L. Wang and Y. Zhu, *Langmuir*, 2012, 28, 8418-8425.

- 424 39. A. S. K. Kumar, S. S. Kakan and N. Rajesh, *Chem. Eng. J.*, 2013, 230,
425 328-337.
- 426 40. U. K. Garg, M. P. Kaur, V. K. Garg and D. Sud, *J. Hazard. Mater.*, 2007, 140,
427 60-68.
- 428 41. C. Moreno-Castilla, M. A. Álvarez-Merino, M. V. López-Ramón and J.
429 Rivera-Utrilla, *Langmuir*, 2004, 20, 8142-8148.
- 430 42. X. J. Hu, Y. G. Liu, G. M. Zeng, S. H. You, H. Wang, X. Hu, Y. M. Guo, X. F.
431 Tan and F. Y. Guo, *J. Colloid Interface Sci.*, 2014, 435, 138-144.
- 432 43. A. K. Giri, R. Patel and S. Mandal, *Chem. Eng. J.*, 2012, 185-186, 71-81.

Fig. 1. The proposed scheme for the formation of DCTA/E/MGO: (Step 1) oxidation of natural graphite to graphite oxide, followed by ultrasonication; (Step 2) preparation of MGO by loading magnetic nanoparticles on the GO surface through chemical coprecipitation method; (Step 3) preparation of DCTA-E solution; (Step 4) formation of DCTA/E/MGO by grafting DCTA-E onto the MGO surface.

Fig. 2. (a) and (b) FESEM images of DCTA/E/MGO; (c) and (d) TEM images of DCTA/E/MGO.

Fig. 3. Nitrogen adsorption –desorption isotherms (a) and pore size distribution (b) of MGO and DCTA/E/MGO; (c) and (d) XRD patterns of GO, MGO and DCTA/E/MGO; (e) FT-IR spectra of MGO and DCTA/E/MGO; (f) XPS wide-scan of MGO and DCTA/E/MGO; (g) and (h) C1s XPS spectra of MGO and DCTA/E/MGO.

Fig. 4. (a) Time-dependent Cr(VI) sorption on DCTA/E/MGO at three different concentrations (10, 20 and 40 mg/L); (b) Pseudo-first-order sorption kinetics; (c) Pseudo-second-order sorption kinetics; (d) Intraparticle diffusion kinetics ($\text{pH} = 3.0 \pm 0.1$, $T = 30\text{ }^\circ\text{C}$, $t = 24\text{ h}$).

Fig. 5. Langmuir and Freundlich non-linear plots of sorption isotherms for Cr(VI) onto DCTA/E/MGO at 15, 30 and 45 °C. The solid lines are Langmuir model simulation, and the dashed lines are Freundlich model simulation ($\text{pH} = 3.0 \pm 0.1$, $t = 24\text{ h}$).

Fig. 6. (a) pH profile of Cr(VI) sorption on DCTA/E/MGO and MGO; (b) Effect of ionic strength on Cr(VI) sorption ($C_{\text{Cr(VI)}}^{\text{initial}} = 20\text{ mg/L}$, $T = 30\text{ }^\circ\text{C}$, $t = 24\text{ h}$).

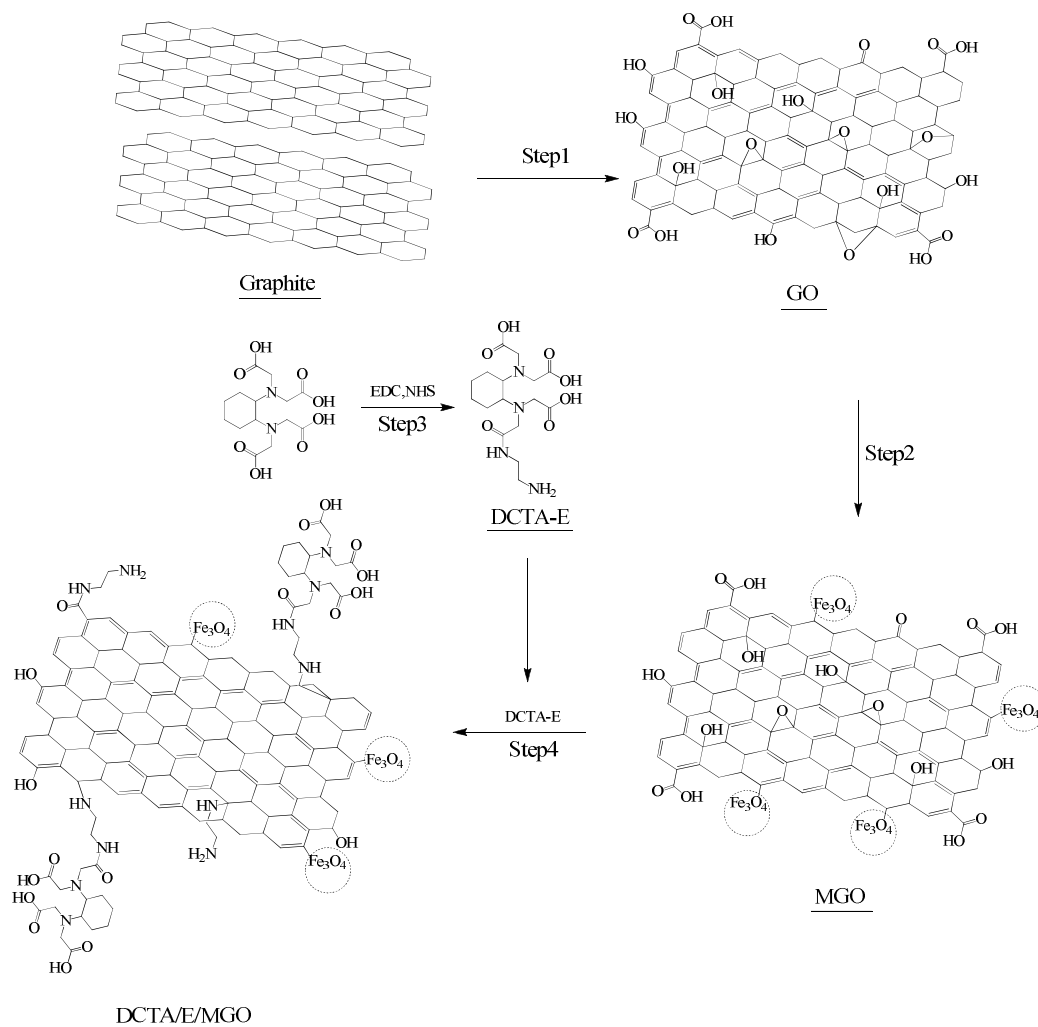


Fig. 1. The proposed scheme for the formation of DCTA/E/MGO: (Step 1) oxidation of natural graphite to graphite oxide, followed by ultrasonication; (Step 2) preparation of MGO by loading magnetic nanoparticles on the GO surface through chemical coprecipitation method; (Step 3) preparation of DCTA-E solution; (Step 4) formation of DCTA/E/MGO by grafting DCTA-E onto the MGO surface.

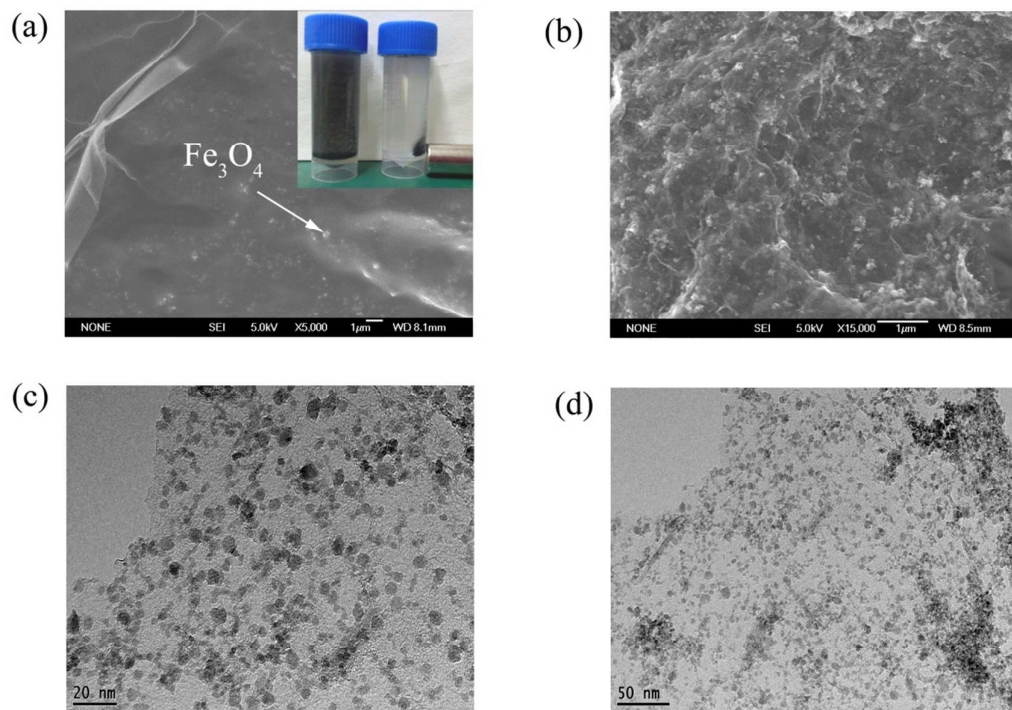


Fig. 2. (a) and (b) FESEM images of DCTA/E/MGO; (c) and (d) TEM images of DCTA/E/MGO.

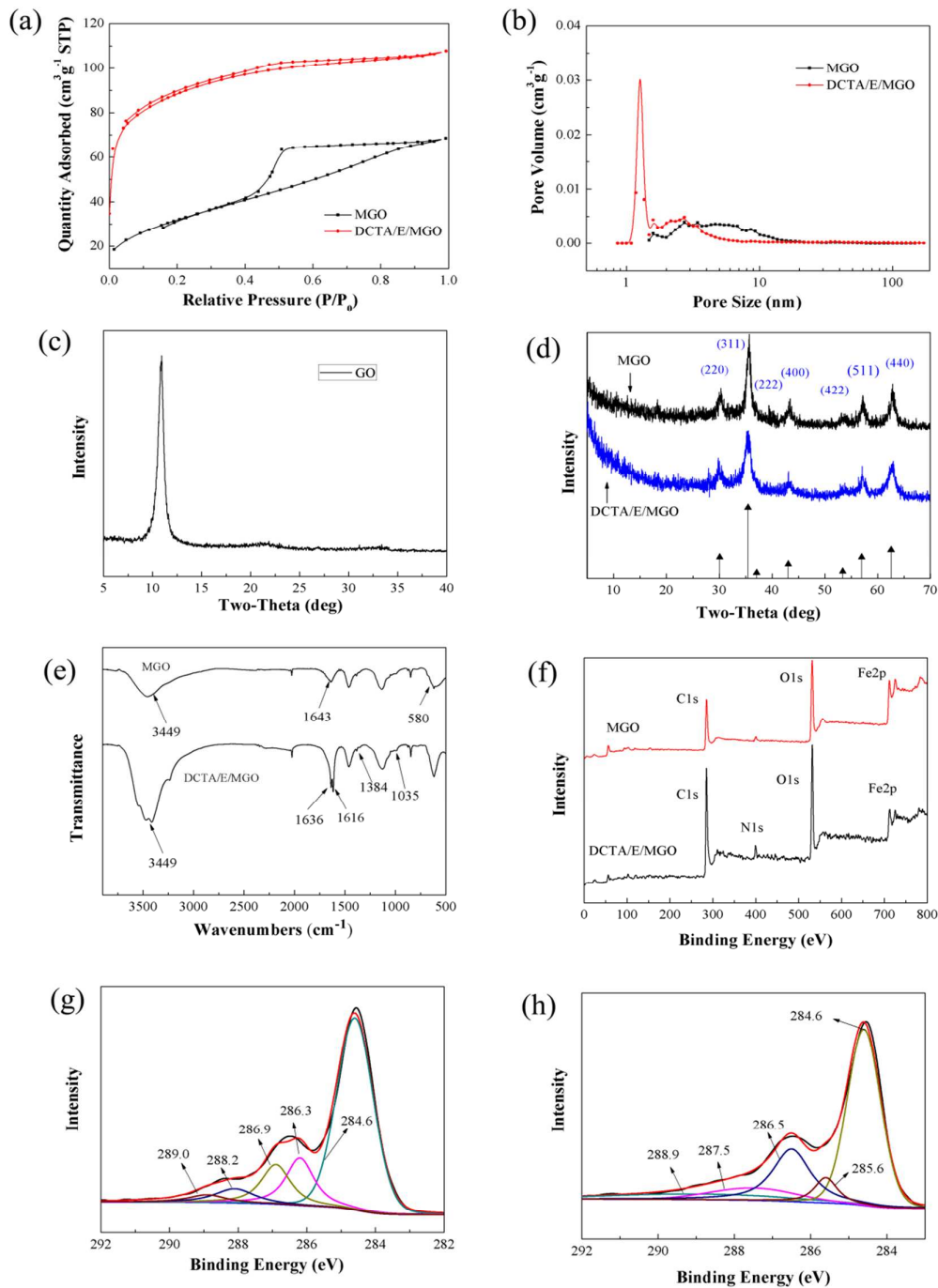


Fig. 3. Nitrogen adsorption–desorption isotherms (a) and pore size distribution (b) of MGO and DCTA/E/MGO; (c) and (d) XRD patterns of GO, MGO and DCTA/E/MGO; (e) FT-IR spectra of MGO and DCTA/E/MGO; (f) XPS wide-scan of MGO and DCTA/E/MGO; (g) and (h) C1s XPS spectra of MGO and DCTA/E/MGO

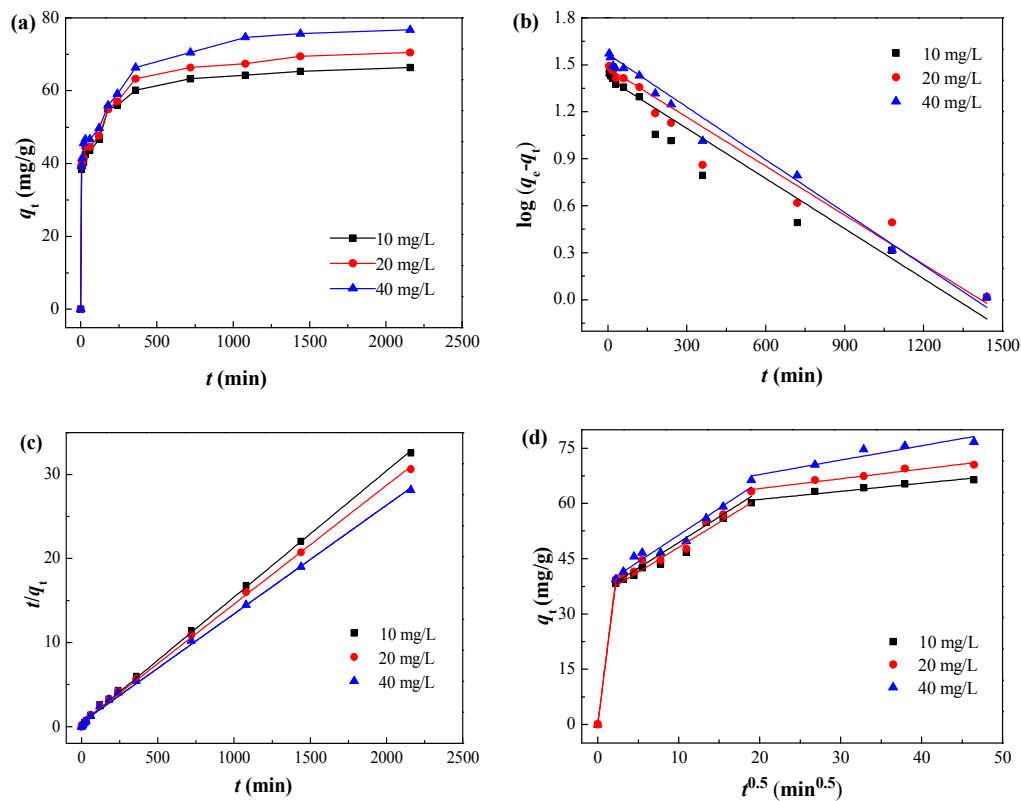


Fig. 4. (a) Time-dependent Cr(VI) sorption on DCTA/E/MGO at three different concentrations (10, 20 and 40 mg/L); (b) Pseudo-first-order sorption kinetics; (c) Pseudo-second-order sorption kinetics; (d) Intraparticle diffusion kinetics (pH = 3.0 \pm 0.1, $T = 30$ $^{\circ}\text{C}$, $t = 24$ h).

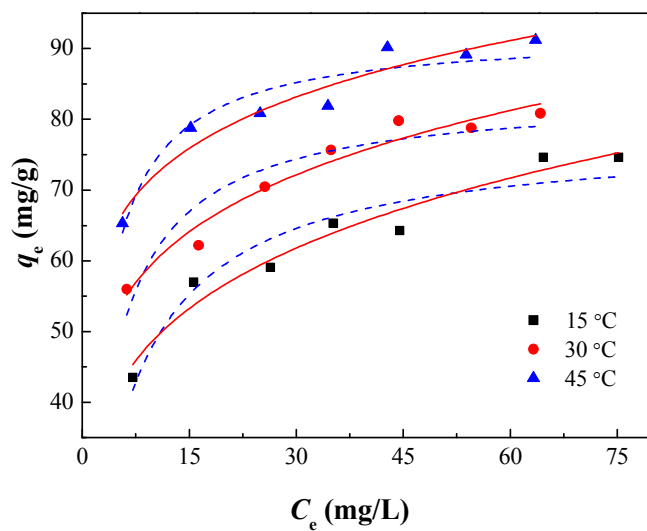


Fig. 5. Langmuir and Freundlich non-linear plots of sorption isotherms for Cr(VI) onto DCTA/E/MGO at 15, 30 and 45 °C. The dashed lines are Langmuir model simulation, and the solid lines are Freundlich model simulation (pH = 3.0 ± 0.1, t = 24 h).

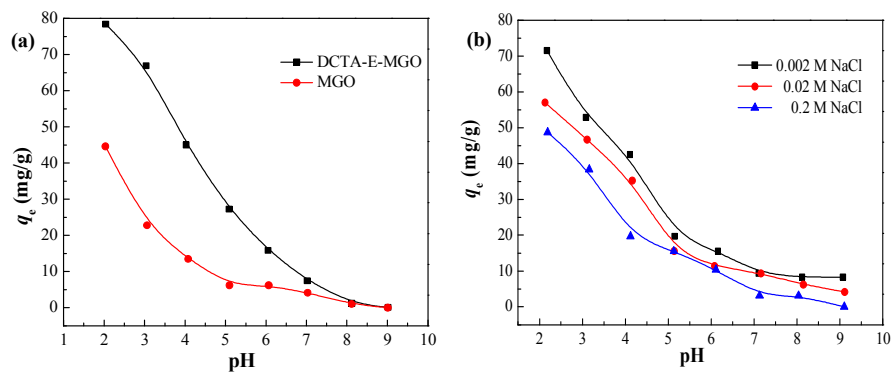


Fig. 6. (a) pH profile of Cr(VI) sorption on DCTA/E/MGO and MGO; (b) Effect of ionic strength on Cr(VI) sorption ($C_{\text{Cr(VI) initial}} = 20 \text{ mg/L}$, $T = 30 \text{ }^\circ\text{C}$, $t = 24 \text{ h}$).

Tale 1 Kinetic parameters for the adsorption of Cr(VI) onto DCTA/E/MGO.

Kinetic parameter		10 mg/L	20 mg/L	40 mg/L
		$q_{e,exp} = 66.34$	$q_{e,exp} = 70.49$	$q_{e,exp} = 76.71$
Pseudo-first-order model	k_1 (1/min)	2.46×10^{-3}	2.40×10^{-3}	2.58×10^{-3}
	$q_{e,1}$ (mg/g)	25.95	30.12	36.94
	R^2	0.894	0.911	0.955
Pseudo-second-order model	k_2 (g/mg min)	5.92×10^{-4}	4.68×10^{-4}	3.55×10^{-4}
	$q_{e,2}$ (mg/g)	66.53	70.72	77.28
	R^2	0.999	0.998	0.998

Table 2 Parameters for Langmuir and Freundlich isotherm models at different temperatures.

T(K)	Langmuir model			Freundlich model		
	q_{\max} (mg/g)	K_L (L/mg)	R^2	K_F (L/mg)	n	R^2
288.15	77.75	0.163	0.900	29.78	4.66	0.950
303.15	83.66	0.267	0.861	40.33	5.84	0.953
318.15	92.27	0.401	0.892	53.07	7.57	0.933

Tale 3 Thermodynamic parameters of Cr(VI) adsorption on DCTA/E/MGO.

Temperature (K)	$\ln K^{\circ}$	ΔG° (kJ/mol)	ΔH° (kJ/mol)	ΔS° (J/K mol)	R^2
288.15	0.511	-1.224	7.65	30.86	0.978
303.15	0.696	-1.754			
318.15	0.811	-2.145			